

Maximising Histopathology Segmentation using Minimal Labels via Self-Supervision

Zeeshan Nisar^{a,*}, Thomas Lampert^a

^a*ICube, University of Strasbourg, CNRS (UMR 7357), France*

Abstract

Histopathology, the microscopic examination of tissue samples, is essential for disease diagnosis and prognosis. Accurate segmentation and identification of key regions in histopathology images are crucial for developing automated solutions. However, state-of-art deep learning segmentation methods like UNet require extensive labels, which is both costly and time-consuming, particularly when dealing with multiple stainings. To mitigate this, multi-stain segmentation methods such as MDS1 and UDAGAN have been developed, which reduce the need for labels by requiring only one (source) stain to be labelled. Nonetheless, obtaining source stain labels can still be challenging, and segmentation models fail when they are unavailable. This article shows that through self-supervised pre-training—including SimCLR, BYOL, and a novel approach, HR-CS-CO—the performance of these segmentation methods (UNet, MDS1, and UDAGAN) can be retained even with 95% fewer labels. Notably, with self-supervised pre-training and using only 5% labels, the performance drops are minimal: 5.9% for UNet, 4.5% for MDS1, and 6.2% for UDAGAN, compared to their respective fully supervised counterparts (without pre-training, using 100% labels). The code is available from https://github.com/zeeshanisar/improve_kidney_glomeruli_segmentation [to

*Corresponding author

Email address: nisar@unistra.fr (Zeeshan Nisar)

be made public upon acceptance].

Keywords: Digital pathology, Deep learning, Stain transfer, Multi-stain segmentation, Stain-invariance, Self-supervised learning, Data scarcity, Kidney glomeruli segmentation

1. Introduction

Histopathology deals with the microscopic examination of tissue to diagnose and detect various diseases and abnormalities. It relies heavily on different stainings to reveal different cell types and structures. Approaches to integrate information from different stainings focus on specific tissue structures as reference points [1]. For instance, the information necessary to study the inflammatory response to a pathology is the distribution of immune cells (e.g. macrophages or lymphocytes) in relation to important organ structures (e.g. glomeruli for the kidney or lobules for the breast).

To automate this, these structures must be detected (segmented) in each tissue section across different stains. This task, referred to as single-stain segmentation, typically employs supervised deep learning algorithms, such as UNet [2], provided that large amount labels are available for each stain (domain¹). However, labelling medical data sets is complex, can require expert knowledge, and be subject to privacy concerns, leading to a scarcity of labels.

To overcome these challenges, various stain transfer based multi-stain segmentation methods have been developed that are trained using labels from only one (source) stain. The current state-of-the-art (SOTA) approaches in this field include: Multi-Domain Supervised 1 (MDS1), which allows the application of a segmentation model trained on a source stain to multiple target stains by translating them to source stain; and (b) Unsupervised Domain Augmentation using Generative Adversarial Networks (UDAGAN),

¹In this study, the terms “stain” and “domain” are equivalent.

an approach to train a single stain-invariant segmentation model on multiple stains but using labels from only the source stain. These methods achieve results comparable to the fully supervised UNet (as will be seen later in this study).

While effective, these methods rely on substantial amounts of source stain labelled data, which can be hard to obtain. In parallel, the size of unlabelled medical imaging datasets are increasing, e.g. the advent of whole slide imaging (WSI) scanners has facilitated the production of vast amounts of histopathological image data. The primary focus of this study is to show that this unlabelled data can counteract the effects of a lack of labelled data in segmentation tasks through self-supervised learning (SSL).

SSL learns representations using unlabelled data by designing a pretext task [3], this representation can then be used in various downstream tasks where labelled data is limited. Accordingly, this study focuses on using the state-of-art SSL methods, such as SimCLR [4], BYOL [5], and our proposed extension to CS-CO [6], called HR-CS-CO, that overcomes its stain-specific limitation. Many SSL studies focus on classification, however there is a lack of studies focusing on segmentation, particularly multi-stain segmentation. Therefore, the downstream segmentation tasks studied herein are: (a) single-stain segmentation using UNet; (b) multi-stain segmentation using MDS1; and (c) stain-invariant segmentation, as multi-stain, using UDAGAN.

Notably, this article will show that when pre-trained with SSL and fine-tuning with few labels, performance comparable to fully (100%) supervised models can be obtained with all the above-mentioned tasks. For instance, five UNets fine-tuned with only ~30 labels, each from one of five different stains, achieve an average F_1 score of 0.810 across all stains, compared to 0.869 for their fully supervised counterparts (each trained with 600 labels). Similarly, fine-tuned MDS1 and UDAGAN models achieve average F_1 scores of 0.744 and 0.765 (respectively), across five stains, using only 30 labels from one (source) stain, whereas their respective baselines trained using 600 labels achieve 0.789 and 0.827 respectively. These findings demonstrate that self-supervised

fine-tuned models can approach the performance of fully supervised models, while significantly reducing label requirements.

To achieve this, this study makes the following contributions:

1. Develop a new formulation for CS-CO (a self-supervised pre-text task), called HR-CS-CO, to overcome its stain-specific limitation, thus making it stain independent.
2. Conduct the first comprehensive analysis of SSL’s impact on multi-stain and stain-invariant segmentation, using the use case of kidney glomeruli segmentation to deduce the most appropriate self-supervised approach.
3. Reduce the annotation requirement of single-stain UNet models by 95%.
4. Reduce the annotation requirement of MDS1 for multi-stain segmentation and UDA-GAN for stain-invariant segmentation by more than 95%, meaning a stain-invariant model can be trained from as few as ~30 labelled glomeruli.

These contributions are validated through ~800 experiments using ~25000 GPU hours.

The rest of the article is organised as follows: Section 2 reviews the literature on SSL; Section 3 provides the architectural details of the afore-mentioned self-supervised pre-training methods and downstream segmentation tasks; Section 4 provides an overview of the dataset and explains the training details; Section 5 evaluates the effectiveness of self-supervised pre-training and provide a detailed comparison to their baseline results; Section 6 discusses these results alongside the limitations and potential applications of our study; and finally, Section 7 concludes the article.

2. Self-Supervised Learning

This section presents an overview of SSL methods for visual representation learning, in which designing a pretext task is key. Based on the type of pretext task, existing SSL methods can be categorised into three groups: generative, discriminative, and multi-tasking. For an in-depth review, please see [7].

2.1. Generative Self-supervised Learning

This group of pretext tasks learns representations by either reconstructing the original input or by learning to generate samples. Auto-encoders and generative adversarial networks (GANs) are commonly used to achieve these objectives. Several such tasks have been proposed in the field of computer vision and medical imaging, e.g. context restoration [3], image denoising [8], visual field expansion [9] and image inpainting [10], etc. However, these approaches are computationally expensive, complex, and may not be necessary when the goal is to learn a simple lower-dimensional data representation [4]. Furthermore, they tend to favour low-level features, which are not effective for discriminative downstream tasks [6]. To address this, various discriminative SSL methods have been introduced.

2.2. Discriminative Self-supervised Learning

Earlier development of these methods focused on context based (or predictive) methods, which showed limited success in medical imaging applications despite significant gains in the computer vision domain [7]. This disparity stems from fundamental differences between natural and medical images, including distinct visual patterns, textures, lighting conditions, and scales. To this end, contrastive learning has emerged as a powerful discriminative approach in both computer vision and medical imaging, particularly in digital histopathology [11, 12]. It learns representations by comparing pairs of input samples to maximise the similarity between similar (positively-paired) samples and minimising it between dissimilar (negatively-paired) samples. Positive pairs are created by augmenting an input image and negative pairs by selecting different images. As such, the positive pairs preserve global features, which encourages the model to discard irrelevant features and focus on learning representations that are discriminative and robust. Notable approaches to this are Contrastive Predictive Coding [13], A Simple Framework for Contrastive Learning of Visual Representations (SimCLR) [4], and Bootstrap Your Own Latent (BYOL) [5] etc.

2.3. *Multi-tasking/Hybrid Self-supervised Learning*

This group is increasing in popularity, in which multiple self-supervised tasks are unified or integrated individually. This can increase the robustness of the representations by reducing bias inherent in individual self-supervised pre-text tasks. Moreover, integrating different approaches to SSL (predictive, generative, and contrastive) improves the model’s ability to capture both low-level and high-level features to simultaneously address multiple objectives. For instance, Graham et al. [14] used multi-tasking to achieve disease classification and segmentation in the same framework. Zhang et al. [15] combine predictive and contrastive SSL tasks and Koohbanani et al. [16] combined multiple predictive tasks. Similarly, Yang et al. [6] and Yu et al. [17] combined generative and discriminative tasks to extract more robust representations.

3. **Methods**

3.1. *Self-Supervised Pre-training*

This study uses three approaches to self-supervised pre-training: SimCLR [4], BYOL [5] and CS-CO [6]. SimCLR is selected due to its widespread adoption in histopathology related downstream tasks [11, 12]. While SimCLR’s performance heavily depends on augmentation and the number of negative pairs, demanding huge computing resources [4, 11], recent methods have shown that negative-pairs are not essential for contrastive learning [5, 18, 19]. One such method is BYOL [5]. The original architectures, as proposed by the authors of SimCLR and BYOL, were used in this study, with details provided in Section 3.1.1 and 3.1.2 respectively. Finally, to assess the benefits of hybrid SSL strategies, a novel extension to CS-CO [6] is included. This extension (presented in Section 3.1.3) overcomes its stain specific formulation (it was proposed for the H&E stain) and is called HR-CS-CO.

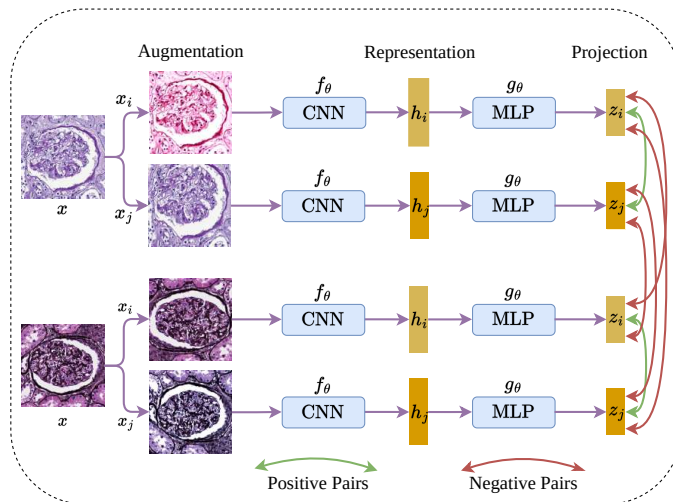


Fig. 1: Overview of the SimCLR architecture inspired by [4, 12].

3.1.1. SimCLR

SimCLR [4] learns representations by maximising the agreement between two augmented views of the same image via contrastive loss in the latent space. As shown in Fig. 1, the framework starts with a probabilistic data augmentation module f_{aug} that generates two positively correlated views, x_i and x_j , of a given data sample x . A set of base augmentations [4] are adopted (using the Albumentations library [20] and parameters from [11]), including random cropping and resizing with a large scale range of (0.2 – 1.0), flipping, grey-scale, Gaussian blur, and random colour distortions. Based on the findings of Stacke et al. [11], two additional augmentations were used, grid distort and grid shuffle, which have demonstrated their effectiveness for histopathology related applications. The augmented views, x_i and x_j are then transformed into their corresponding representations, h_i and h_j by employing a convolutional neural network (CNN) base encoder f_θ , where θ is the weight parameters.

Subsequently, a projection head g_θ consisting of a multi-layer perceptron (MLP) is employed to map the extracted representations into a lower embedding space in

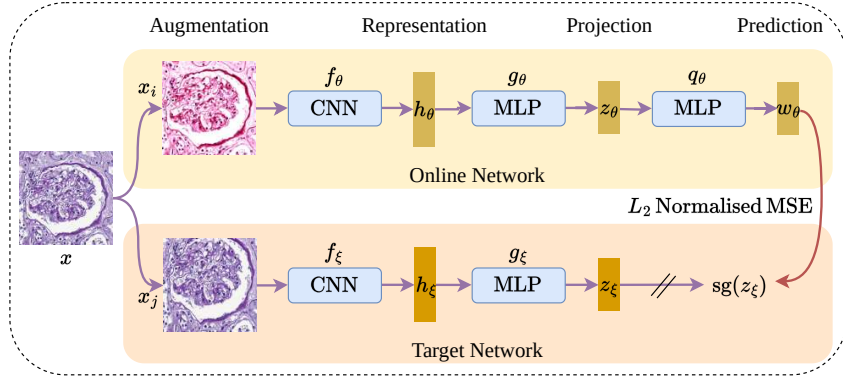


Fig. 2: Overview of BYOL architecture inspired by Grill et al. [5].

which the contrastive loss is applied. The MLP comprises two dense layers with ReLU activation for the first layer; and linear activation for the second layer to obtain $z_i = g_\theta(h_i)$ and $z_j = g_\theta(h_j)$ respectively. In [4], it was observed that comparing z_i and z_j was more effective for learning representations than directly comparing h_i and h_j . Finally, as suggested by the authors of SimCLR, to optimise the entire network the NT-Xent (the normalised temperature-scaled cross-entropy loss) function is defined, such that

$$\ell_{i,j} = -\log \frac{\exp(\text{sim}(z_i, z_j)/\tau)}{\sum_{k=1}^{2N} \mathbb{1}_{[k \neq i]} \exp(\text{sim}(z_i, z_k)/\tau)}, \quad (1)$$

where τ is the temperature parameter that weights different samples and facilitates learning from hard negative samples and $\mathbb{1}$ is the indicator function. The term $\text{sim}(z_i, z_j) = z_i^T z_j / \|z_i\| \|z_j\|$ represents the dot product between ℓ_2 normalised z_i and z_j , which corresponds to the cosine similarity. This loss functions aims to maximise the agreement between positive pairs of augmented images, while minimising it for other images in the same batch (negative pairs). In each training step with a batchsize of $2N$, each augmented image has one positive and $2(N - 1)$ negative pairs.

3.1.2. BYOL

Bootstrap Your Own Latent Representation (BYOL) is an implicit contrastive learning approach introduced by Grill et al. [5]. It does not rely on negative pairs and is more robust to the choice of augmentations, resulting in superior performance compared to other contrastive methods. The core idea of BYOL is to iteratively bootstrap the network’s output to serve as a target for an enhanced representation. To achieve this, BYOL employs two neural networks, Online and Target, which interact and learn from each other. As depicted in Fig. 2, the Online network is a trainable network comprising a CNN based encoder f_θ , an MLP based projection head g_θ , and a prediction head q_θ . On the other hand, the Target network is a non-trainable network that is randomly initialised. It has the same architecture as the Online network, but has a different set of weight parameters ξ . The Target network provides the regression targets, used to train the Online network, and its parameters ξ are updated through an exponential moving average of the Online parameters θ . Considering a target decay rate $\tau \in [0, 1]$, the following update is carried out after each training step:

$$\xi \leftarrow \tau\xi + (1 - \tau)\theta. \tag{2}$$

To train the BYOL network, a data augmentation module f_{aug} is used to generate two distinct augmented views x_i and x_j from the input image x . This module incorporates the same augmentations as described for SimCLR. The Online network processes the first augmented view x_i and outputs a representation h_θ , a projection z_θ , and a prediction w_θ . Similarly, the Target network outputs a representation h_ξ , and a target projection z_ξ from the second augmented view x_j . Notably, the prediction head is solely applied to the Online network, resulting in an asymmetric architecture between the Online and Target pipelines. Following that, both w_θ and z_ξ are normalised using ℓ_2 norm and then

fed into a mean squared error (MSE) loss function, such that

$$\mathcal{L}_{\theta,\xi} = \|\bar{w}_\theta - \bar{z}_\xi\|_2^2 = 2 - 2 \cdot \frac{\langle w_\theta, z_\xi \rangle}{\|w_\theta\|_2 \cdot \|z_\xi\|_2}. \quad (3)$$

The loss $\mathcal{L}_{\theta,\xi}$ is made symmetrical by separately feeding x_j to the Online network and x_i to the Target network. This allows the computation of another loss function $\tilde{\mathcal{L}}_{\theta,\xi}$. During each training step, a stochastic optimisation step is performed to minimise $\mathcal{L}_{\theta,\xi}^{BYOL} = \mathcal{L}_{\theta,\xi} + \tilde{\mathcal{L}}_{\theta,\xi}$ with respect to θ only, while ξ remains unaffected by applying a stop-gradient (*sg*) as shown in Fig. 2.

3.1.3. CS-CO

CS-CO [6] is a hybrid SSL method, designed particularly for Haematoxylin and Eosin (H&E) stained histopathology images. It contains two stages: cross-stain prediction and contrastive learning. The cross-stain prediction, which is a generative task, captures low-level general features, e.g. nuclei morphology and tissue texture, that are valuable for histopathology analysis [6]. To facilitate this, stain-separation [21] is applied to H&E stained images to extract the single-dye channels, Haematoxylin (H_{ch}) and Eosin (E_{ch}). Afterwards, cross-stain prediction is employed to learn the relationship between H_{ch} and E_{ch} , using two separate auto-encoders, H2E and E2H, where H2E predicts E_{ch} from H_{ch} , and vice-versa.

Nevertheless, CS-CO has certain limitations, restricting its broader applicability. For example, histopathological images often use different staining protocols and reagents to highlight different tissue structures (e.g. PAS, Jones H&E, Sirius Red, CD68, and CD34, as used in this study). The stain separation method integral to CS-CO struggles with ImmunoHistochemical (IHC) stains [21]. Particularly, it fails to accurately extract the individual H_{ch} and DAB_{ch} (Diaminobenzidine) from CD68. Furthermore, in some cases, histopathological stains contain more than two dyes, e.g. Jones H&E, where CS-CO’s stain-separation approach would yield three separate channels— J_{ch} (Jones), H_{ch} ,

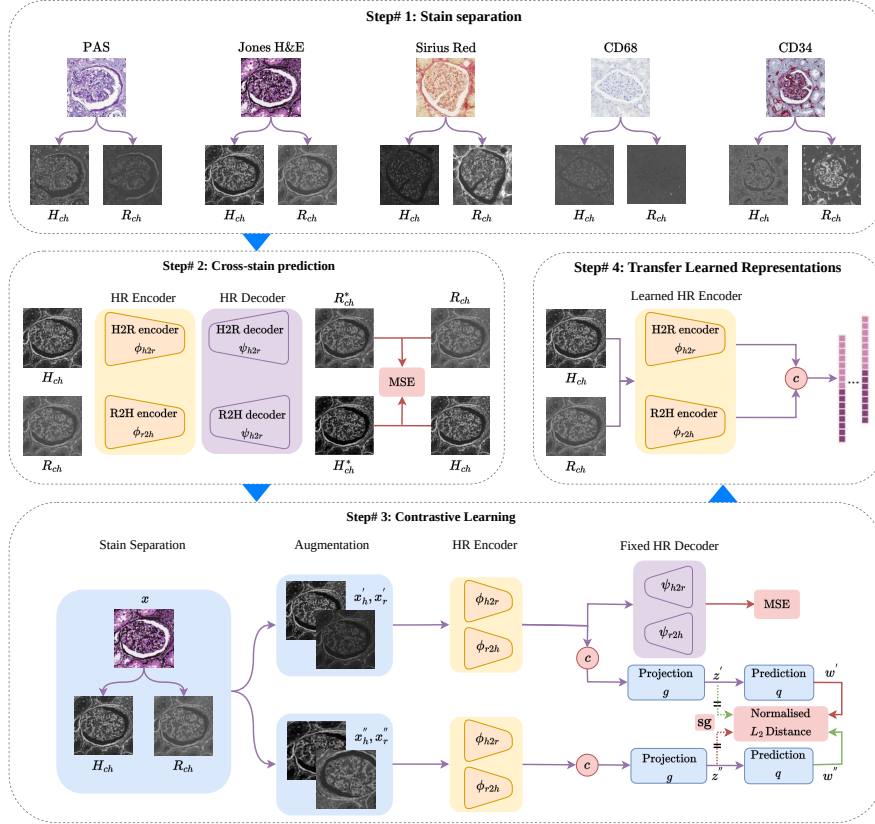


Fig. 3: Overview of the proposed HR-CS-CO architecture. In Step# 1, stain-separation is applied to separate the H_{ch} and R_{ch} from each each stain. In Step# 2, the cross-stain prediction is employed as a generative task, learning to predict H_{ch} from R_{ch} and R_{ch} from H_{ch} . Lastly, in Step# 3, contrastive learning is used as discriminative task on the augmented views of H_{ch} and R_{ch} to learn the final representations. Here, the weights for ϕ and ψ are initialised to those learnt during cross-stain prediction (i.e. Step #2), thereby combining the strength of generative and discriminative learning.

and E_{ch} —which cannot be handled in CS-CO’s architecture.

To address these limitations and extend the applicability of CS-CO across multiple stainings, we propose to modify its stain-separation strategy as outlined in Figure 3. Particularly, we exploit the fact that Haematoxylin is often used as a counterstain in histopathology, and therefore exists in many stains. This was first exploited by Lampert et al. [1] as a strategy for stain invariant segmentation. Here, however, we use it to extract a common Haematoxylin channel, H_{ch} , which highlights cell nuclei, via im-

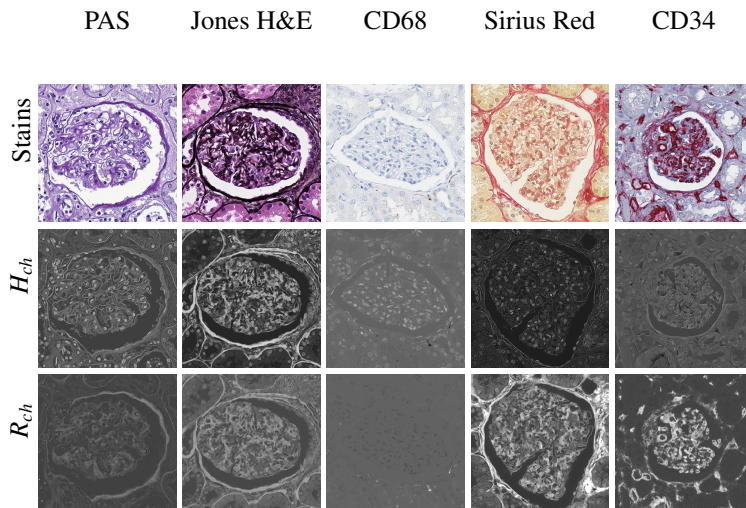


Fig. 4: Visualisation of Haematoxylin (H_{ch}) and Residual (R_{ch}) channels extracted from each of the stains used in this study.

age deconvolution [22]. The remaining information is retained as a ‘Residual’ channel (R_{ch}) as illustrated in Fig. 3, step #1, and Fig. 4, capturing tissue structure highlighted by the other stain components, such as glycogen, collagen, macrophages, and endothelial cells, etc, depending on the staining used. Therefore, all stain (containing H_{ch}) can be included by modelling them as H_{ch} and R_{ch} . In the rest of the article, we refer to this modified version of CS-CO as HR-CS-CO.

Moving forward, in the cross-stain prediction stage, two separate auto-encoders H2R and R2H are trained as shown in Fig. 3 (Step #2). H2R learns to predict R_{ch} from H_{ch} , and R2H performs the inverse task. Both share the same architecture but have different weights. For simplicity, ϕ_{h2r} and ψ_{h2r} is used to represent the encoder and decoder for H2R (and similarly for R2H). Additionally, the combination of ϕ_{h2r} and ϕ_{r2h} , and ψ_{h2r} and ψ_{r2h} , are denoted as the HR encoder and decoder respectively. The mean square error (MSE) loss is computed to evaluate the dissimilarity between the real (H_{ch}, R_{ch}) and predicted (H_{ch}^*, R_{ch}^*) images, such that

$$\mathcal{L}_{cs} = \left(H_{ch} - H_{ch}^*\right)^2 + \left(R_{ch} - R_{ch}^*\right)^2, \quad (4)$$

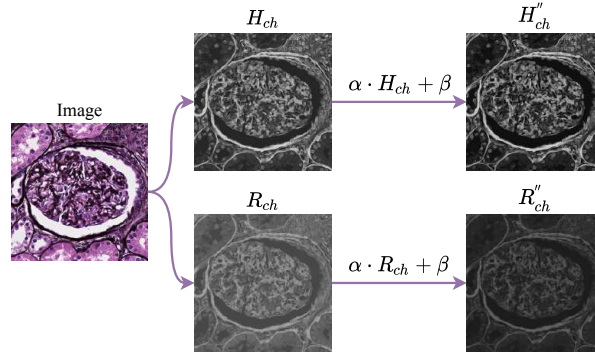


Fig. 5: Stain-variation augmentation. From left to right: the process begins by decomposing an Image into its corresponding Haematoxylin (H_{ch}) and Residual (R_{ch}) channels. Subsequently, each channel undergoes individual modification using a random factor α and bias β . The modified versions are represented as H'_{ch} and R'_{ch} .

where $R_{ch}^* = \psi_{h2r}(\phi_{h2r}(H_{ch}))$ and $H_{ch}^* = \psi_{r2h}(\phi_{r2h}(R_{ch}))$. This makes the two-branched auto-encoder sensitive to low-level features [6].

Next, contrastive learning is used in Step# 3 (as a final step) to learn high-level discriminative features. The model is reorganised into a Siamese architecture [18], consisting of the HR encoder (ϕ), a projection head (g), and a prediction head (q), in which the parameters of the two branches are shared. Both g and q are multi-layer perceptrons (MLP) with the same architecture. To prevent mode collapse, the HR decoder (ψ), is retained in one branch as a non-trainable regulator. Instead of employing random initialisation, the weights for ϕ and ψ are initialised to those learnt during cross-stain prediction (i.e. Step #2), thereby combining the strength of general low-level and discriminative high-level features.

During contrastive learning, H_{ch} and R_{ch} are extracted from a given input image x to give (x_h, x_r) and augmentation (f_{aug}) is applied to generate two distinct augmented views of each data sample: (x'_h, x'_r) and (x''_h, x''_r) . f_{aug} includes various augmentations such as flipping, random cropping and resizing, and Gaussian blur. Since the images are grey-scale, colour-based augmentations are not used, however stain variation is included as an additional augmentation, where the pixel intensities of each extracted

channel are modified by a random factor $\alpha \in [-0.25, 0.25]$ and bias $\beta \in [-0.05, 0.05]$.

These values were chosen as they result in realistic output, see Fig. 5.

Subsequently, each augmented pair is fed into the Siamese network and encoded by ϕ_{h2r} and ϕ_{r2h} . The outputs are pooled and concatenated to form a single vector, which is processed by g to obtain (z', z'') and q to obtain (w', w'') . The symmetrised loss is

$$\mathcal{L}_{co} = \frac{1}{2} \|\bar{w}' - \bar{z}''\|_2^2 + \frac{1}{2} \|\bar{w}'' - \bar{z}'\|_2^2, \quad (5)$$

where \bar{w}' , \bar{w}'' , \bar{z}' , and \bar{z}'' are the ℓ_2 normalised versions of w' , w'' , z' , and z'' , respectively. This encourages w' and w'' to be similar to z'' and z' (respectively). Before computing the loss, the stop-gradient (sg) is applied to z' and z'' . This sg step introduces a necessary asymmetry in gradient flow, which, when combined with the symmetrised loss, allows robust and diverse feature learning. During contrastive learning, the frozen pre-trained HR decoder (ψ) continues to use the outputs of the HR encoder (ϕ) for image reconstruction. To avoid collapse, the HR encoder must maintain the necessary information for image reconstruction, by satisfying Equation 4. As a result, the total loss is formulated as $\mathcal{L}_{sco} = \mathcal{L}_{cs} + \gamma \mathcal{L}_{co}$, where γ is the weight coefficient.

3.2. Downstream Segmentation Tasks

Once a model has been pre-trained using one of the self-supervised pre-training methods mentioned above, it can be fine-tuned for various downstream tasks. The primary aim of this study is to investigate the use of these pre-training methods to reduce the need of labels for several segmentation tasks, (a) UNet [2], (b) MDS1 [23], and (c) UDAGAN [24], as shown in Fig. 6. The original architectures as proposed by the authors were used, with details provided below. Additional details on combining these with pre-training are presented in Section 4.2.

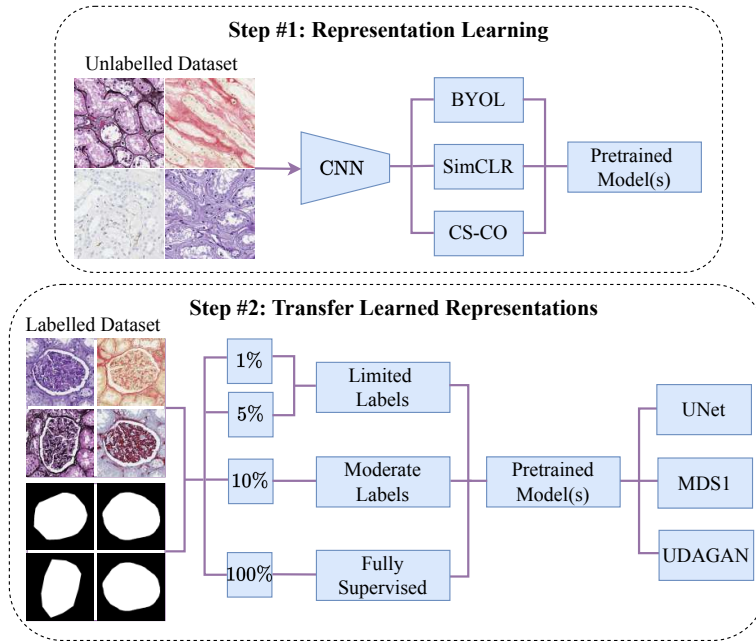


Fig. 6: Workflow of our study. Step #1: Different SSL methods are applied to learn representations from a large unlabelled dataset. Step # 2: The learned representations are then refined by fine-tuning on a small labelled data for different histopathology related segmentation tasks.

3.2.1. UNet

UNet [2] is a highly effective CNN architecture, see Fig. 7, that has shown remarkable efficacy in segmenting biomedical images, specifically for glomeruli segmentation [1, 25]. It adopts an encoder-decoder structure, forming a U-shaped network, which effectively handles both local and global information. The encoder path, also known as the contracting path, comprises repetitive blocks, each encompassing two consecutive 3×3 convolutions followed by ReLU activation and a max-pooling layer. Conversely, the decoder path, or expanding path, gradually upsamples the feature maps using 2×2 transposed convolution layers. Subsequently, the corresponding feature map from the contracting path is cropped and concatenated with the up-sampled feature map, followed by two consecutive 3×3 convolutions and a ReLU activation. Finally, a 1×1 convolution is applied to reduce the feature map to the desired number of channels

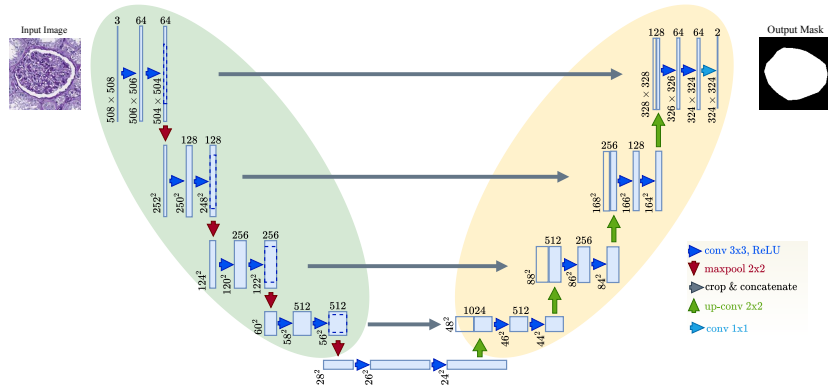


Fig. 7: Overview of the UNet architecture.

(classes), generating the segmentation map. The cropping step is necessary since pixels at the edges contains less contextual information and therefore should be discarded.

3.2.2. *MDS1 and UDAGAN*

These are stain transfer based multi-stain segmentation approaches, that use labels from the source (S) stain, which is PAS in our case, and eliminate the need for labels in the target (T) stains (herein these are Jones H&E, Sirius Red, CD68, CD34). Stain transfer is achieved using a cycle-consistent generative adversarial network (CycleGAN) [26]. For both MDS1 and UDAGAN, a separate CycleGAN model ($M_{\text{cycGAN}}^{S \leftrightarrow T}$) is trained to translate between the S and each T stain, i.e. from $S \rightarrow T$ and $T \rightarrow S$, see Fig. 8(a). The architectural descriptions for CycleGAN are detailed in [26].

In MDS1 [23], see Fig. 8(b), a UNet segmentation model (M_{unet}^S), as detailed above, is trained using the source stain and its labels. Then, during testing, the target stain is translated to match the source, referred to as the ‘fake S’, and M_{unet}^S is applied on ‘fake S’ to obtain segmentation masks.

In contrast, UDAGAN [24] combines stain augmentation and adaptation to create a stain-invariant model that can be directly applied to multiple stains without test-time translation. Specifically, CycleGAN models ($M_{\text{cycGAN}}^{S \rightarrow T}$) are used to augment the labelled source stain by randomly translating images to one of the target stains. Since

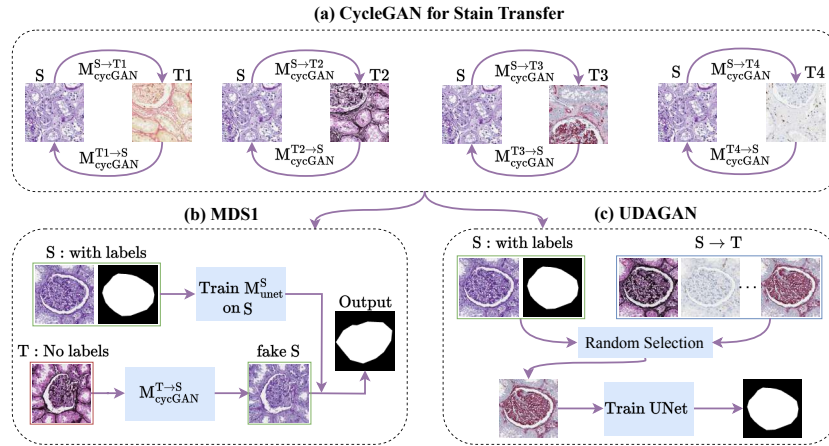


Fig. 8: Overview of MDS1 and UDAGAN architecture.

translation does not change the image’s structure, see Fig. 8(c), it’s ground truth is still valid. As such, several annotated samples from all available stains are presented to the UNet, resulting in a single stain-invariant model able to segment several target stains.

4. Experimental Setup

4.1. Dataset

The findings presented herein were evaluated for kidney glomeruli segmentation using a private histopathology dataset provided by the Hannover Medical School. Tissue samples were collected from 10 patients who had tumor nephrectomy due to renal carcinoma. The renal tissue was selected as distant as possible from the tumors to represent largely normal renal glomeruli. However, certain samples exhibited varying degrees of pathological modifications, such as complete or partial displacement of functional tissue by fibrotic changes (“sclerosis”) indicating normal age-related changes or the renal effects of general cardiovascular comorbidity (e.g. cardiac arrhythmia, hypertension, arteriosclerosis). Using the Ventana Benchmark Ultra automated staining tool, the paraffin-embedded samples were sliced into 3 μ m thick sections and stained with ei-

Table 1: Training data with different percentages of labelled glomeruli for each staining.

% of Labels	Stainings				
	PAS	Jones H&E	CD68	Sirius Red	CD34
1%	6	5	5	6	5
5%	33	31	26	32	28
10%	66	62	52	65	56
100%	662	621	526	651	565

ther Jones H&E, PAS, Sirius Red, and two immunohistochemistry markers (CD34, and CD68). An Aperio AT2 scanner was used to capture whole slide pictures at 40 magnification (a resolution of 0.253 m / pixel), resulting in WSIs ranging from 37k×25k to 107k×86k pixels. Pathologists annotated and verified all of the glomeruli in each whole slide image (WSI) by labelling them with Cytomine [27]. The dataset was split into 4 training, 2 validation, and 4 test patients. The level-of-detail used is 1 (corresponding to 20× magnification) with a patch size of 508 × 508 pixels, as to contain a glomeruli with its surrounding area.

4.1.1. Self-Supervised Pre-Training

The dataset for self-supervised pre-training is extracted from the training and validation WSIs in an unsupervised manner (uniformly sampled). To be representative of each patient, 15,000 (training) and 1,000 (validation) patches were extracted from each stain, resulting in 75,000 training and 5,000 validation patches.

4.1.2. Downstream Segmentation Tasks

Glomeruli segmentation is framed as a two class problem: glomeruli (pixels belonging to glomeruli), and tissue (pixels outside a glomerulus). The performance of the trained models is evaluated by segmenting the full test patient WSIs from each stain. The number of glomeruli present in the test stainings are: PAS - 1092; Jones H&E - 1043; Sirius Red - 1049; CD34 - 1019; CD68 - 1046.

UNet – Following Ciga et al. [12], multiple splits of the overall dataset were created

that contains different percentages of labelled data (1%, 5%, 10%, 100%) taken from the training patients of each stain (see Table 1). Additionally, seven times more tissue (i.e. non-glomeruli) patches were included to account for the variability observed in non-glomeruli tissue. Similar to Stacke et al. [11], a validation dataset is used to select the best model based on the loss. The number of glomeruli present in the validation stainings are: PAS - 588; Jones H&E - 590; Sirius Red - 576; CD34 - 595; CD68 - 521.

MDS1 & UDAGAN – To train the respective CycleGAN models, 5000 patches are randomly extracted from the training WSIs of each stain (PAS being the source, and the rest the targets). Additionally, when fine-tuning the pre-trained MDS1 and UDAGAN models, the same splits as used for the UNet were used, but only those of the PAS stain, see Table 1 (1st column).

4.2. Training Details

4.2.1. Self-Supervised Pre-training

SimCLR and BYOL use CNN based encoders however, CS-CO relies on a CNN-based auto-encoder. The UNet offers SOTA performance in glomeruli segmentation [1, 25] and therefore its encoder was used for SimCLR and BYOL and encoder and decoder for CS-CO. In each of these networks, the extracted representations are subsequently projected into a lower-dimensional space using a multi-layer perceptron (MLP). The best trained model is selected based on the self-supervised validation dataset. Each SSL network was trained once due to computational and time constraints. The training details for each self-supervised pre-training method are detailed below.

SimCLR: The training setup proposed in the original paper [4] was used. Recently, Stacke et al. [11] has shown that smaller batch sizes are preferable when using SimCLR in histopathology, particularly when dealing with few classes, and therefore a batch size of 256 was used, since this reduces the risk of false negatives. This also allowed

the higher resolution (i.e. 508×508 pixels) of histopathological images to be used. Following [11], we trained SimCLR for 200 epochs.

BYOL: A similar training procedure as described in the original BYOL paper [5] was used. The absence of negative samples in BYOL’s training paradigm allows it to sustain performance parity with SimCLR despite using smaller batch sizes. A batch size of 256 was chosen and the model was trained for 200 epochs. Since BYOL can be susceptible to poor initialisation, the encoder uses batch-normalisation (BN).

HR-CS-CO: Since the concentration of the H_{ch} can vary between different stainings, we train separate HR-CS-CO models for each. The two training stages (see Section 3.1) have the following training strategies: Cross-stain prediction, the model is trained for 100 epochs with a batch size of 32 using the Adam optimiser with initial learning rate (LR) of 0.001, which, based on the validation loss and a patience of 10 epochs, is reduced by a factor of 0.1; Contrastive learning, the model is trained again for 50 epochs and a batch size of 128 using the Adam optimiser with LR of 0.001 and a weight decay of 10^{-6} . To prevent over-fitting, early stopping is used in both stages.

4.2.2. Downstream Segmentation Tasks

As is common, the validation loss (see Section 4.1.2) is used to select the final model [6, 11, 12]. This is, however, a hindrance in histopathology (and medical imaging in general) since it requires additional labels. Thus, additional experiments were performed without a validation set by selecting the best model based on the training loss. The training details for downstream tasks (UNet, MDS1, and UDAGAN) and the strategy to combine the pre-trained features from each of the self-supervised pre-trained method are detailed below.

UNet: The UNet is trained for 250 epochs (following Vasiljević et al. [24]) using a batch size of 8 and a learning rate of 0.0001. All patches are standardised to $[0, 1]$ and normalised by the mean and standard deviation of the training set. The same augmen-

tation as used by Lampert et al. [1] are applied with an independent probability of 0.5 (batches are augmented ‘on the fly’), that is: elastic deformation ($\sigma = 10$, $\alpha = 100$); random rotation in the range $[0^\circ, 180^\circ]$, random shift sampled from $[-205, 205]$ pixels, random magnification sampled from $[0.8, 1.2]$, and horizontal/vertical flip; additive Gaussian noise with $\sigma \in [0, 2.55]$; Gaussian filtering with $\sigma \in [0, 1]$; brightness, colour, and contrast enhancements with factors sampled from $[0.9, 1.1]$; stain variation by colour deconvolution [28], α sampled from $[-0.25, 0.25]$ and β from $[-0.05, 0.05]$. To integrate the benefits of the knowledge gained from self-supervised pre-training, the encoder component of the UNet architecture is initialised with the weights learned during pre-training (i.e. with SimCLR, BYOL, or CS-CO). Five different repetitions of the UNet model were trained for each stain and for each split of labelled data.

MDS1: MDS1 requires both a UNet and CycleGAN network to be trained. The UNet is trained as described above. The key difference being that it uses only labelled splits of the source stain (PAS). For CycleGAN, the network architecture and loss weights ($w_{cyc} = 10$, $w_{id} = 5$) are taken from the original paper [26]. To deal with large patch sizes (i.e. above 256×256 pixels), a translation network with nine ResNet blocks is employed. The model is trained for 50 epochs, with a LR of 0.0002 using the Adam optimiser, and a batch size of 1. Starting from the 25th epoch, the LR is linearly decayed to 0, and the weights for cycle-consistency (w_{cyc}) and identity (w_{id}) are halved. In all experiments, the translation model from the final epoch is used. To reduce model oscillation, Shrivastava et al. [29]’s strategy is adopted that updates the discriminator using the 50 previously generated samples. To account for random variations, the CycleGAN network was trained three times per target stain, and five UNets were trained per CycleGAN (resulting in 15 repetitions for each split of the source stain labels).

UDAGAN: The training of UDAGAN is similar to MDS1, incorporating both UNet and CycleGAN networks. Specifically, in the first step, CycleGAN network is trained for each target stain, enabling the translation from $S \rightarrow T$. Subsequently, a training

patch from S stain is translated into randomly selected T stain (with a probability of $\frac{N-1}{N}$, where N is the number of stains) using the pre-trained CycleGAN network(s). Thus, all available stains (including the S stain) are presented to the UNet model with equal probability, $\frac{1}{N}$, forcing the network to learn stain invariant features. The training details for CycleGAN and UNet are the same as those outlined in MDS1. One UDAGAN model is trained for each split of the S stain labels and repeated five times.

5. Results

In this section, the pre-trained models are evaluated for each downstream task (UNet, MDS1, and UDAGAN) in two different settings: fixed-features and fine-tuning. In the fixed-feature setting, the pre-trained weights are frozen to assess the quality of the learned representations from self-supervised pre-trained models, using the same hyperparameters as used for baseline models. When fine-tuning, the pre-trained weights are updated. To determine the optimal hyperparameters for fine-tuning, a separate hyperparameter study was conducted using 1%, and 5% splits of labelled data and the performance was evaluated on the validation set for each task and pre-training method. Five learning rate values, logarithmically spaced between 0.0001 and 0.1, were tested. Additionally, two different settings for weight decay were examined: one with a value of 10^{-4} and one without any weight decay. The learning rate was reduced by a factor of 0.1 at the 90th percentile of training. Based on these experiments, the best hyperparameters were selected, and the fine-tuned models were re-trained for all label splits. The F_1 score is used as the evaluation metric and the results are presented on a separate unseen test set (as outlined in Section 4.1.2).

Fully supervised models were trained to establish baselines for different label splits, including 100% labels. It was found that the fine-tuned models consistently outperform fixed-feature models, and therefore only fine-tuned results are shown here (fixed-feature results are in [Appendix A](#)).

Table 2: A comparison of various self-supervised pre-training methods and respective baselines (randomly initialised without any pre-training) for the downstream tasks of UNet, MDS1, and UDAGAN using various splits of labelled data. For UNet, the labels have been used for all stains, while for MDS1 and UDAGAN, the labels for only source (PAS) stain are used. The evaluation is conducted on an independent, unseen test dataset using F₁ score. Each F₁ score is the average of five different training repetitions (standard deviations are in parentheses). The highest F₁ score for each stain, across different label splits, is in italics, while the overall highest F₁ score averaged across all stains is in bold.

Downstream Tasks	Label Splits	Pre-training	Test Stains					Average
			PAS	Jones H&E	CD68	Sirius Red	CD34	
UNet	1%	None (Baseline)	0.015 (0.031)	0.000 (0.000)	0.000 (0.000)	0.000 (0.000)	0.253 (0.059)	0.054 (0.018)
		SimCLR	<i>0.673 (0.021)</i>	0.519 (0.040)	0.407 (0.015)	0.472 (0.037)	0.652 (0.018)	0.544 (0.026)
		BYOL	0.660 (0.018)	<i>0.635 (0.055)</i>	<i>0.625 (0.042)</i>	<i>0.561 (0.044)</i>	<i>0.686 (0.030)</i>	0.633 (0.038)
		HR-CS-CO	0.154 (0.044)	0.188 (0.067)	0.048 (0.083)	0.337 (0.082)	0.463 (0.017)	0.238 (0.058)
	5%	None (Baseline)	0.546 (0.084)	0.593 (0.080)	0.370 (0.188)	0.707 (0.055)	0.782 (0.041)	0.600 (0.090)
		SimCLR	<i>0.852 (0.019)</i>	<i>0.760 (0.017)</i>	0.599 (0.039)	0.618 (0.042)	<i>0.802 (0.011)</i>	0.726 (0.026)
		BYOL	0.768 (0.036)	0.746 (0.076)	<i>0.736 (0.033)</i>	<i>0.721 (0.051)</i>	<i>0.800 (0.047)</i>	0.754 (0.049)
		HR-CS-CO	0.756 (0.079)	0.628 (0.086)	0.533 (0.067)	0.406 (0.067)	0.707 (0.037)	0.606 (0.067)
	10%	None (Baseline)	0.730 (0.017)	0.792 (0.024)	0.643 (0.053)	<i>0.788 (0.022)</i>	0.827 (0.063)	0.756 (0.036)
		SimCLR	<i>0.867 (0.019)</i>	0.813 (0.012)	0.690 (0.057)	0.696 (0.060)	<i>0.838 (0.007)</i>	0.781 (0.031)
		BYOL	0.794 (0.047)	<i>0.823 (0.054)</i>	<i>0.729 (0.052)</i>	0.722 (0.044)	0.776 (0.057)	0.769 (0.051)
		HR-CS-CO	0.807 (0.058)	0.748 (0.098)	<i>0.729 (0.040)</i>	0.711 (0.074)	0.791 (0.026)	0.757 (0.059)
	100%	None (Baseline)	<i>0.894 (0.021)</i>	0.840 (0.029)	0.836 (0.031)	0.865 (0.019)	<i>0.888 (0.015)</i>	0.865 (0.024)
		SimCLR	0.884 (0.003)	<i>0.873 (0.007)</i>	0.840 (0.011)	<i>0.881 (0.007)</i>	0.867 (0.027)	0.869 (0.011)
		BYOL	0.867 (0.009)	0.842 (0.035)	0.818 (0.036)	0.847 (0.012)	0.874 (0.021)	0.850 (0.022)
		HR-CS-CO	0.843 (0.033)	0.855 (0.015)	<i>0.872 (0.006)</i>	0.842 (0.023)	0.870 (0.011)	0.856 (0.018)
MDS1	1%	None (Baseline)	—	0.030 (0.066)	0.024 (0.054)	0.039 (0.086)	0.036 (0.079)	0.032 (0.071)
		SimCLR	—	<i>0.615 (0.015)</i>	<i>0.403 (0.031)</i>	<i>0.594 (0.026)</i>	<i>0.614 (0.028)</i>	0.556 (0.025)
		BYOL	—	0.516 (0.041)	0.363 (0.027)	0.525 (0.047)	0.494 (0.031)	0.474 (0.037)
		HR-CS-CO	—	0.326 (0.025)	0.224 (0.045)	0.359 (0.050)	0.384 (0.035)	0.323 (0.039)
	5%	None (Baseline)	—	0.711 (0.032)	0.526 (0.041)	0.685 (0.031)	0.613 (0.050)	0.634 (0.038)
		SimCLR	—	<i>0.798 (0.005)</i>	0.534 (0.015)	0.767 (0.008)	<i>0.729 (0.016)</i>	0.707 (0.011)
		BYOL	—	0.713 (0.051)	<i>0.538 (0.047)</i>	0.733 (0.032)	0.605 (0.061)	0.647 (0.048)
		HR-CS-CO	—	0.760 (0.028)	0.335 (0.084)	<i>0.773 (0.015)</i>	0.607 (0.044)	0.619 (0.043)
	10%	None (Baseline)	—	0.776 (0.017)	<i>0.575 (0.025)</i>	0.778 (0.023)	0.656 (0.030)	0.696 (0.024)
		SimCLR	—	<i>0.784 (0.026)</i>	0.541 (0.029)	0.752 (0.040)	<i>0.722 (0.016)</i>	0.700 (0.028)
		BYOL	—	0.706 (0.063)	0.541 (0.060)	0.731 (0.084)	0.650 (0.043)	0.657 (0.062)
		HR-CS-CO	—	0.771 (0.037)	0.433 (0.059)	<i>0.804 (0.041)</i>	0.633 (0.033)	0.660 (0.042)
	100%	None (Baseline)	—	0.849 (0.017)	<i>0.683 (0.043)</i>	0.870 (0.009)	<i>0.754 (0.008)</i>	0.789 (0.032)
		SimCLR	—	0.826 (0.033)	0.638 (0.056)	0.836 (0.034)	0.712 (0.030)	0.753 (0.038)
		BYOL	—	0.833 (0.032)	0.632 (0.042)	0.864 (0.028)	0.652 (0.066)	0.745 (0.042)
		HR-CS-CO	—	<i>0.863 (0.017)</i>	0.614 (0.067)	<i>0.878 (0.018)</i>	0.730 (0.040)	0.771 (0.036)
UDAGAN	1%	None (Baseline)	0.000 (0.000)	0.000 (0.000)	0.000 (0.000)	0.000 (0.000)	0.000 (0.000)	0.000 (0.000)
		SimCLR	0.477 (0.015)	0.403 (0.025)	0.261 (0.053)	0.408 (0.010)	0.518 (0.016)	0.413 (0.024)
		BYOL	<i>0.647 (0.062)</i>	<i>0.504 (0.083)</i>	<i>0.401 (0.099)</i>	<i>0.513 (0.088)</i>	<i>0.598 (0.064)</i>	0.533 (0.079)
	5%	None (Baseline)	0.669 (0.038)	0.498 (0.056)	0.352 (0.056)	0.618 (0.072)	0.692 (0.024)	0.566 (0.049)
		SimCLR	0.719 (0.018)	0.616 (0.020)	0.524 (0.014)	0.632 (0.015)	0.716 (0.015)	0.641 (0.016)
		BYOL	<i>0.815 (0.027)</i>	<i>0.730 (0.071)</i>	<i>0.603 (0.028)</i>	<i>0.732 (0.028)</i>	<i>0.726 (0.055)</i>	0.721 (0.042)
	10%	None (Baseline)	0.816 (0.031)	0.687 (0.014)	0.614 (0.019)	0.750 (0.069)	0.770 (0.022)	0.727 (0.031)
		SimCLR	0.781 (0.013)	0.712 (0.013)	0.606 (0.015)	0.706 (0.026)	0.768 (0.012)	0.715 (0.016)
		BYOL	<i>0.834 (0.035)</i>	<i>0.767 (0.051)</i>	<i>0.654 (0.040)</i>	<i>0.742 (0.090)</i>	<i>0.781 (0.037)</i>	0.755 (0.051)
	100%	None (Baseline)	<i>0.901 (0.011)</i>	0.856 (0.036)	0.705 (0.031)	0.873 (0.025)	0.799 (0.035)	0.827 (0.027)
		SimCLR	0.892 (0.008)	<i>0.866 (0.018)</i>	<i>0.777 (0.013)</i>	<i>0.888 (0.015)</i>	<i>0.844 (0.003)</i>	0.853 (0.011)
		BYOL	0.883 (0.019)	0.854 (0.039)	0.722 (0.051)	0.818 (0.068)	0.792 (0.036)	0.814 (0.042)

The results presented in Table 2 indicate that, in the majority of limited label scenarios (1%, 5%), the fine-tuned models consistently outperformed the baselines, while with moderate (10%) and fully labelled (100%) data, they result in similar or better performance across all stains.

On average, in the limited label cases, which are equivalent to 5–6 (1%) and 26–33 (5%) labelled glomeruli per stain, the fine-tuned UNet models significantly outperform the respective baseline UNet models (see last column). This outperformance is not uniform over all stains however, notably Sirius Red and CD34 with 5% labels do benefit from pre-training but not as considerably as the other stains. For some stains, it can be observed that pre-training with 100% labels can even outperform the baseline fully supervised models, however, the benefits are not evident when averaging over all stains. As our goal is to find a labelling level that minimises labelling effort while maximising performance, 5% labels offers a good balance between the two (10% giving only a small increase in performance, while 1% a considerable drop). At this level of labelling, a 11% drop in performance is observed with BYOL pre-trained UNet in comparison to the fully (100%) supervised model. This highlights that the number of labels required for training can be reduced by 95%. If SSL had not been used in this case, a 26.9% drop in performance would have been observed (5th row, last column of Table 2).

In MDS1 multi-stain segmentation, the same pattern can be observed. Using 1% and 5% labels (but in this case only from the source, PAS, stain) results in a considerable average performance increase over the baseline models. Focusing on 5% labels, SimCLR pre-training enables MDS1 to achieve an average F_1 score of 0.707, which is only 8.2% lower than the 100% supervised MDS1 baseline (0.789), while reducing the labelling requirement by 95%. Moreover, this is only 5% lower than the best average UNet single-stain performance with pre-training, which requires labels for all stains, whereas MDS1 requires them for only the source stain.

Table 3: Downstream task performance with 5% training labels, without a validation set. UNet, 5% labels are used for all stains, MDS1 and UDAGAN, 5% labels are used for only source, PAS, stain. The evaluation is conducted on test set. Each F₁ score is the average of five different training repetitions (standard deviations in parentheses). Highest F₁ score for each stain is in italics, overall highest F₁ score averaged across all stains is in bold.

Downstream Tasks	Pre-training	Test Stains					Average
		PAS	Jones H&E	CD68	Sirius Red	CD34	
UNet	SimCLR	<i>0.812 (0.019)</i>	0.795 (0.034)	0.575 (0.146)	0.612 (0.066)	0.810 (0.020)	0.720 (0.057)
	BYOL	0.786 (0.020)	<i>0.839 (0.025)</i>	<i>0.771 (0.027)</i>	<i>0.788 (0.021)</i>	<i>0.870 (0.003)</i>	0.810 (0.019)
	HR-CS-CO	0.777 (0.032)	0.695 (0.092)	0.428 (0.086)	0.425 (0.094)	0.700 (0.060)	0.605 (0.072)
MDS1	SimCLR	—	0.787 (0.016)	0.608 (0.015)	0.770 (0.021)	<i>0.704 (0.022)</i>	0.717 (0.018)
	BYOL	—	<i>0.813 (0.037)</i>	<i>0.646 (0.038)</i>	<i>0.823 (0.037)</i>	0.695 (0.038)	0.744 (0.037)
	HR-CS-CO	—	0.776 (0.013)	0.251 (0.051)	0.812 (0.007)	0.599 (0.026)	0.609 (0.024)
UDAGAN	SimCLR	0.402 (0.193)	0.389 (0.078)	0.000 (0.000)	0.072 (0.120)	0.359 (0.260)	0.244 (0.130)
	BYOL	<i>0.850 (0.008)</i>	<i>0.822 (0.021)</i>	<i>0.650 (0.029)</i>	<i>0.815 (0.026)</i>	<i>0.771 (0.011)</i>	0.765 (0.022)

This trend continues in the stain invariant UDAGAN model’s results, where on average pre-training and fine-tuning with 1% and 5% labels (again, for only the source stain) considerably outperforms the baselines in all stains. HR-CS-CO pre-training is not evaluated as UDAGAN is a stain-invariant single-model multi-stain segmentation approach and HR-CS-CO is trained separately for each stain. In this case, we observe a 10.6% performance drop when fine-tuning with 5% labels (and pre-training with BYOL) compared to the 100% supervised baselines. If the model had been trained in a fully supervised manner with this amount of labels, a 26.1% drop would have been observed, thus fine-tuning is able to minimise the impact of the lack of labels.

A visual confirmation of these findings is shown in Fig. 9, in which glomeruli segmentation maps (for models trained with 5% labels) for each stain are presented.

5.1. Omitting Validation Data

As shown above, a balance between minimising labels and maximising performance is achieved using 5% labels. Nevertheless, when training the final models, the results were obtained using a fully labelled validation set. Therefore, Table 3 evaluates whether the validation set is necessary or whether this labelling requirement can also be reduced. It is shown that in many cases, the performance without a validation set outperforms that obtained when using a labelled validation set. This is explained by the

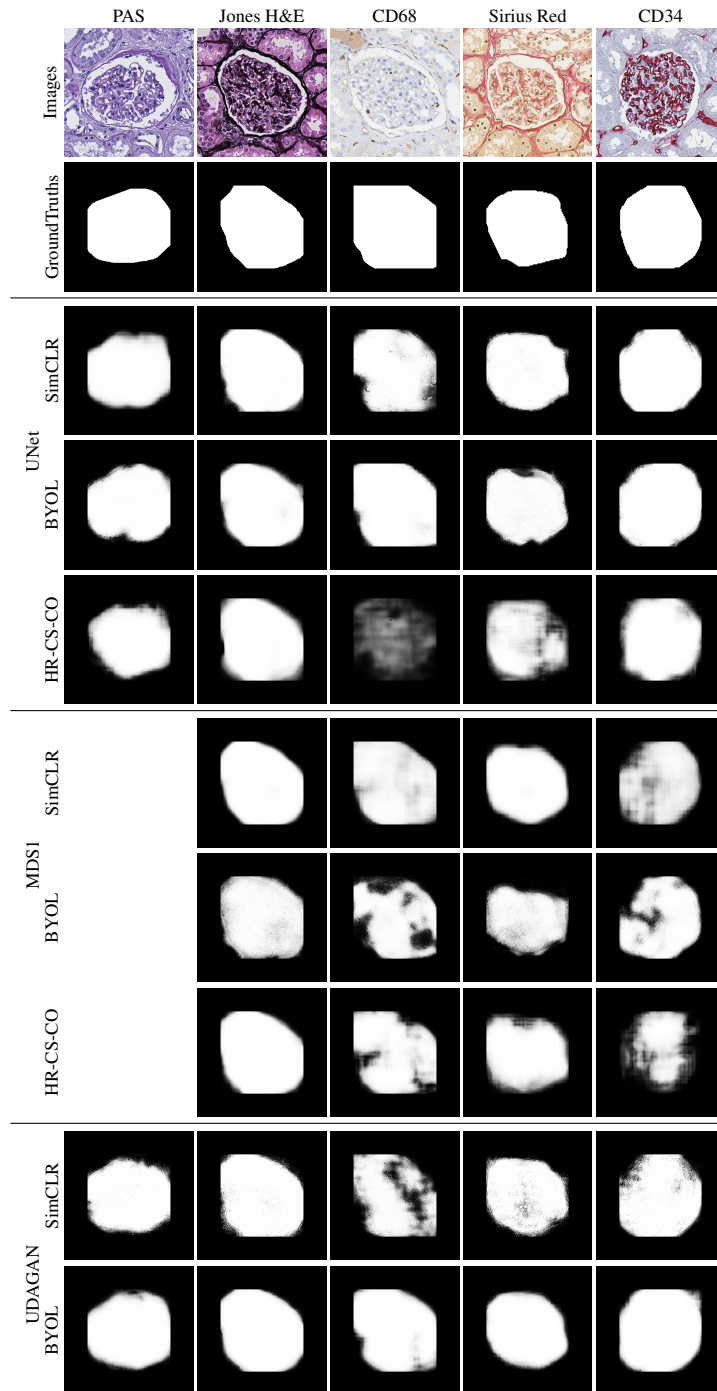


Fig. 9: Visual comparison between predicted glomeruli segmentation maps and real ground-truths for each test stain using fine-tuned UNet, MDS1, and UDAGAN models (trained with 5% labels).

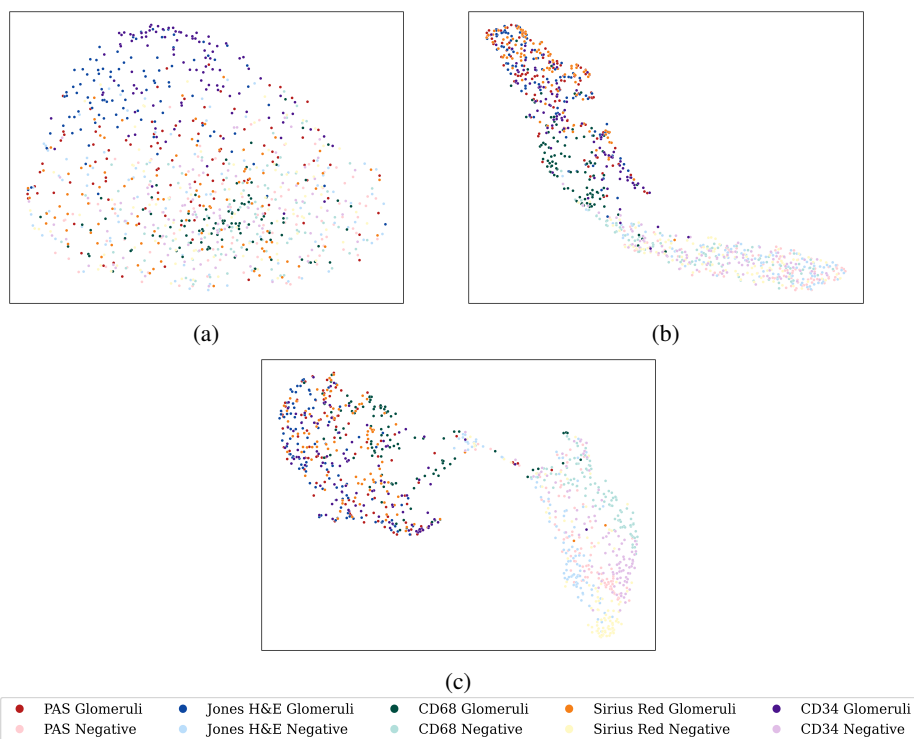


Fig. 10: Two-dimensional UMAP embeddings of the representations learned by: (a) SimCLR and (b) BYOL based UDAGAN models, trained without a validation set, and (c) SimCLR UDAGAN with a 5% labeled validation set. Models randomly chosen, representations sampled from the penultimate convolutional layer, 100 patches per stain per class from the unseen test set. Each point is a patch from the respective class and staining.

fact that in the dataset used, there is a lower domain shift (measured by following [30]) between the train and test set distributions, which is 0.0655 (averaged across all stains), compared to the train and validation set distributions, 0.1857. This allows the models trained without validation data to outperform (on the test data) those selected using the validation loss. Although, this behaviour is specific to datasets with the above-mentioned characteristic, it only affects the difference in performance between the two experimental settings and not the findings themselves. Let us imagine that there were a lower domain shift between the validation and training sets, in this case removing the validation set would only eliminate the increase in performance observed here. It therefore does not invalidate the findings presented herein, that the validation set can

be removed to further minimise labelling requirements.

With SimCLR and UDAGAN, however, a considerable drop in performance is observed. This is likely because of overfitting in the absence of validation data. The model is trained in two stages: (1) pre-training using SimCLR on original image patches; (2) translation (using CycleGAN models) from PAS to all other stains during fine-tuning. During the second stage, imperceptible noise caused by the CycleGAN transfer [30] is introduced into the training patches. This causes a domain shift between the training data and test images, reducing performance. This is exacerbated by the absence of a validation set, which would normally prevent overfitting to this ‘noisy’ training data. In contrast, BYOL is not affected because it uses batch-normalisation, which helps to stabilise the training process and prevent overfitting the noisy inputs. This can be visualised in Fig. 10, where there is a noticeable lack of class boundary between test glomeruli and negative patches when training SimCLR-UDAGAN without a validation set, see Fig. 10(a). Such a boundary exists in the BYOL-UDAGAN representation without validation data, see Fig. 10(b), and a SimCLR-UDAGAN trained with 5% validation labels, see Fig. 10(c) (for comparison, this model achieves an average F_1 score of 0.686, vs. 0.244 without the validation set).

6. Discussion

The previous section showed the effectiveness of SSL in combating a lack of labelled segmentation data in histopathology, approaching fully-supervised performance (e.g. with BYOL pre-training) in both single-stain UNet and multi-stain UDAGAN models (e.g. with ~30 labels per training stain).

We can observe however that not all self-supervised learning approaches are equal. When fewer labels are available (1% and 5%), general computer vision (CV) approaches such as SimCLR and BYOL perform best. Even though HR-CS-CO is specifically designed for histopathology, it only becomes competitive and/or outperforms

the CV approaches when provided with moderate (10%) to larger amounts of labelled data. It is particularly successful when applied to the CD68 stain, outperforming even the baseline models. CD68 is an immunohistochemical stain in which haematoxylin highlights the main structural component and specific immune cells are highlighted in brown. It is therefore particularly suited to an approach such as HR-CS-CO. There are many other similar immunohistochemical stainings, and more complicated double stainings (e.g. CD3-CD68, CD3-CD163, CD3-CD206, etc [31]) that should be suitable for such an approach (including the H&E stain CS-CO was originally developed for). In some of the other stains used in this study (e.g. Sirius Red), it appears that the superposition of staining components (and weak haematoxylin staining) prevents the haematoxylin channel from being efficiently extracted, limiting the effectiveness of HR-CS-CO (the difficulty of extracting this component from Sirius Red has been previously noted in the literature [1]).

The final intended tasks of the pre-trained model often dictate the type of SSL that should be used. In UDAGAN, BYOL consistently outperforms SimCLR, especially with highly limited labels, likely due to its robustness to noise during fine-tuning. Unlike SimCLR, which relies on negative pairs, BYOL uses only positive samples and keeps a moving average for regularisation, making it less sensitive to noisy (i.e. translated) data during fine-tuning [32]. Nevertheless, SimCLR outperforms BYOL in MDS1, despite both being applied to ‘noisy’ translated stains, notably CD68 (MDS1’s UNet is trained on the source stain’s real, noise-free, data making it sensitive to any noise in the target→PAS data during testing [30]). It is known that this is particularly evident in immunohistochemical stainings such as CD68 and CD34 [24, 30], which is confirmed in this study where the noise degrades the performance of all pre-training methods equally, including downstream segmentation.

The role of validation data was shown to strongly impact the success of fine-tuning pre-trained models. Surprisingly, omitting a validation set greatly improved the suc-

cess of fine-tuning, reaching performance levels approaching those of fully supervised models. This means that almost state-of-the-art performance can be achieved while reducing labelling requirements by 95%.

Finally, the benefits of self-supervised pre-training are not just restricted to limited label situations. This study has shown that the performance of fully-supervised stain-invariant models such as UDAGAN can be improved—pre-training the UDAGAN model before fully-supervised training lead to a 2.6% increase in F_1 score. This offers a new SOTA performance in stain-invariant glomeruli segmentation without any architectural nor labelling changes.

Moving away from renal histopathology, these results are consistent with other histopathology studies found in the literature and extend upon existing efforts to reduce the need for extensive manual annotations. Particularly, Prakash et al. [8] showed that for nuclei segmentation in the Broad Bioimage Benchmark Collection dataset, a self-supervised fine-tuned UNet using only 5% labels (32 images) demonstrated only 3% reduction in IoU score compared to a full supervised UNet. Similarly, Punn et al. [33] reported that a self-supervised fine-tuned UNet using 20% labels (134 images) for nuclei segmentation on the Kaggle Datascience Bowl Challenge 2018 dataset only lost 5.1% in F_1 score compared to a fully supervised UNet. Combined with the results presented herein, these demonstrate minimal performance degradation despite significant reductions in label requirements. The findings presented herein, however, go further. Not only do they show the benefit of integrating pre-training into fully-supervised approaches, but also into multi-stain segmentation strategies and removing the need for labelled validation datasets. This more than reduces the labelling requirement to the source stain (a reduction of at least n times, where n is the number of stains to be segmented).

This discussion has already outlined the limitations of HR-CS-CO and so it remains to address SSL limitations in general. Foremost, there is a risk of introducing false

negatives when training SimCLR on datasets with few classes because mini-batches are likely to contain several samples from one class. This can lead to a model that fails to distinguish between semantically “similar” and “dissimilar” images, reducing downstream performance. BYOL, however, overcomes this limitation by not using negative pairs. Moreover, contrastive SSL in general relies on augmentation to create “similar” pairs. As outlined by Garcea et al. [34], medical imaging is sensitive to augmentation since it contains subtle, easily distorted features.

7. Conclusions

This article has shown how to significantly reduce the need for labelled data (>95%) in histopathology image segmentation. To achieve this, self-supervised pre-training techniques— SimCLR, BYOL, and a novel histopathological SSL approach, HR-CS-CO—were used to learn general features from unlabelled data. These features were then fine-tuned for single stain and multi-stain segmentation tasks using UNet, MDS1, and UDAGAN models, making them robust to training scenarios with limited labels.

These approaches demonstrated consistently superior performance compared to their respective baselines, and were able to approach the performance of fully supervised models. These findings underscore the potential and significance of incorporating these advanced learning techniques in histopathology. The results also demonstrated that self-supervised learning combined with fine-tuning is most effective without a validation set, further reducing the labelling requirement. However, some methods, such as SimCLR, are more susceptible to domain shifts and may benefit from some labelled validation data to ensure generalisation.

Furthermore, this study advanced the recent trend in histopathology towards creating multi-stain segmentation models by demonstrating that it is possible to train a stain-invariant segmentation model with as few as ~30 labelled positive patches from one stain. This model closely matches the performance of a fully supervised UNet

trained with ~3000 positive patches.

CRedit authorship contribution statement

ZN: Conceptualisation, Methodology, Software, Validation, Investigation, Visualisation, Writing - original draft. **TL:** Conceptualisation, Data Curation, Supervision, Funding acquisition, Writing - review & editing.

Acknowledgements

Funded by ANR HistoGraph (ANR-23-CE45-0038) and the ArtIC project “Artificial Intelligence for Care” (grant ANR-20-THIA-0006-01), co funded by *Région Grand Est*, Inria Nancy - Grand Est, IHU Strasbourg, University of Strasbourg & University of Haute-Alsace. We acknowledge the ERACoSysMed & e:Med initiatives by BMBF, SysMIFTA (managed by PTJ, FKZ 031L-0085A; ANR, grant ANR-15-CMED-0004), Prof. Cédric Wemmert, and Prof. Friedrich Feuerhake and team at MHH for the high-quality images & annotations: N. Kroenke, N. Schaadt, V. Volk & J. Schmitz. We thank Nvidia, the *Centre de Calcul* (University of Strasbourg) & GENCI-IDRIS (grant 2020-A0091011872) for GPU access.

References

- [1] T. Lampert, et al., Strategies for training stain invariant CNNs, in: ISBI, 2019, pp. 905–909.
- [2] O. Ronneberger, et al., U-Net: Convolutional networks for biomedical image segmentation, in: MICCAI, 2015, pp. 234–241.
- [3] L. Chen, et al., Self-supervised learning for medical image analysis using image context restoration, *Med. Image Anal.* 58 (2019) 101539.

- [4] T. Chen, et al., A simple framework for contrastive learning of visual representations, in: ICML, 2020, pp. 1597–1607.
- [5] J.-B. Grill, et al., Bootstrap your own latent—a new approach to self-supervised learning, *NeurIPS* 33 (2020) 21271–21284.
- [6] P. Yang, et al., CS-CO: A hybrid self-supervised visual representation learning method for H&E-stained histopathological images, *MedIA* 81 (2022) 102539.
- [7] S. Shurrab, et al., Self-supervised learning methods and applications in medical imaging analysis: A survey, *PeerJ Comput. Sci.* 8 (2022) e1045.
- [8] M. Prakash, et al., Leveraging self-supervised denoising for image segmentation, in: ISBI, 2020, pp. 428–432.
- [9] J. Boyd, et al., Self-supervised representation learning using visual field expansion on digital pathology, in: CVPR, 2021, pp. 639–647.
- [10] S.-Y. Hu, et al., Self-supervised pretraining with DICOM metadata in ultrasound imaging, in: PMLR, 2020, pp. 732–749.
- [11] K. Stacke, et al., Learning representations with contrastive self-supervised learning for histopathology applications, *MELBA* 1 (2022) 1–33.
- [12] O. Ciga, et al., Self supervised contrastive learning for digital histopathology, *MLWA* 7 (2022) 100198.
- [13] M. Y. Lu, et al., Semi-supervised breast cancer histology classification using deep multiple instance learning and contrast predictive coding, in: *MedIA*, 2020, p. 113200J.
- [14] S. Graham, et al., One model is all you need: Multi-task learning enables simultaneous histology image segmentation and classification, *MedIA* 83 (2023) 102685.

- [15] Y. Zhang, et al., Twin self-supervision based semi-supervised learning (TS-SSL): Retinal anomaly classification in SD-OCT images, *Neurocomputing* 462 (2021) 491–505.
- [16] N. A. Koohbanani, et al., Self-Path: Self-supervision for classification of pathology images with limited annotations, *IEEE TMI* 40 (2021) 2845–2856.
- [17] H. Yu, et al., Self-supervised multi-task learning for medical image analysis, *Pattern Recognit.* 150 (2024) 110327.
- [18] X. Chen, et al., Exploring simple siamese representation learning, in: *CVPR*, 2021, pp. 15745–15753.
- [19] S. Li, et al., Minent: Minimum entropy for self-supervised representation learning, *Pattern Recognit.* 138 (2023) 109364.
- [20] A. Buslaev, et al., Albumentations: Fast and flexible image augmentations, *Information* 11 (2020) 125.
- [21] A. Vahadane, et al., Structure-preserving color normalization and sparse stain separation for histological images, *IEEE TMI* 35 (2016) 1962–1971.
- [22] A. C. Ruifrok, et al., Quantification of histochemical staining by color deconvolution, *Anal. Quant. Cytol. Histol.* 23 (2001) 291–299.
- [23] M. Gadermayr, et al., Generative adversarial networks for facilitating stain-independent supervised and unsupervised segmentation: A study on kidney histology, *IEEE TMI* 38 (2019) 2293–2302.
- [24] J. Vasiljević, et al., Towards histopathological stain invariance by unsupervised domain augmentation using generative adversarial networks, *Neurocomputing* 460 (2021) 277–291.

- [25] T. de Bel, et al., Automatic segmentation of histopathological slides of renal tissue using deep learning, in: MedIA, 2018, pp. 285–290.
- [26] J.-Y. Zhu, et al., Unpaired image-to-image translation using cycle-consistent adversarial networks, in: ICCV, 2017, pp. 2242–2251.
- [27] R. Marée, et al., Collaborative analysis of multi-gigapixel imaging data using Cytomine, *Bioinformatics* 32 (2016) 1395–1401.
- [28] D. Tellez, et al., Whole-slide mitosis detection in H&E breast histology using PHH3 as a reference to train distilled stain-invariant convolutional networks, *IEEE TMI* 37 (2018) 2126–2136.
- [29] A. Shrivastava, et al., Learning from simulated and unsupervised images through adversarial training, in: CVPR, 2017, pp. 2242–2251.
- [30] Z. Nisar, et al., Towards measuring domain shift in histopathological stain translation in an unsupervised manner, in: ISBI, 2022, pp. 1–5.
- [31] O. Merveille, et al., An automatic framework for fusing information from differently stained consecutive digital whole slide images: A case study in renal histology, *Comput. Methods Programs Biomed* 208 (2021) 106157.
- [32] K.-H. Lee, et al., Compressive visual representations, *NeurIPS* 34 (2021) 19538–19552.
- [33] N. S. Punn, et al., BT-Unet: A self-supervised learning framework for biomedical image segmentation using barlow twins with U-net models, *Machine Learning* 111 (2022) 4585–4600.
- [34] F. Garcea, et al., Data augmentation for medical imaging: A systematic literature review, *Comput. Biol. Med.* 152 (2023) 106391.

Appendix A. Results with Fixed Representations

To evaluate whether self-supervised learning methods are able to learn meaningful representations and generalise to downstream tasks, it is important to use a fixed-feature setting. Therefore, in this setting, the representations learned are used as feature vectors in the downstream tasks of UNet, MDS1, and UDAGAN and the results are provided in Table A.4, evaluated across different splits of labelled data. Since these self-supervised pre-training methods are not explicitly designed for learning representations well-suited for the tasks of UNet, MDS1, and UDAGAN. Consequently, fixed-feature settings exhibit a significant drop in performance when compared to fine-tuned models (as presented in Table 2), and this is particularly noticeable in the case of HR-CS-CO. This highlights the need for a more effective stain separation methods beyond the classical, matrix decorrelation based approach employed in our study. This is why, during fine-tuning, HR-CS-CO’s representation is able to better adapt to the specific characteristics of the downstream task, and therefore compensate for the limitations caused by the loss of information resulting from the stain separation used during training. Nonetheless, it is essential to acknowledge that even though fixed-feature models experience a decline in performance, they show improved results in comparison to baseline models, especially when employing SimCLR and BYOL as pre-trained models. This improvement is particularly evident when the models are subjected to limited labelled data, such as 1% and 5%. Moreover, when provided with moderate (10%) to fully (100%) labelled data, the fixed-feature models approach the performance levels of baseline models. This highlights the effectiveness of self-supervised learning methods in the context of their capacity to learn meaningful representations.

Table A.4: Performance evaluation of various self-supervised learning based UNet methods in a fixed-feature scenario for glomeruli segmentation. The performance is evaluated in terms of segmentation (F_1) score, averaged over five different training repetitions, with the standard deviations presented in parentheses.

Downstream Tasks	Label Splits	Pre-training	Test Stains					Average
			PAS	Jones H&E	CD68	Sirius Red	CD34	
UNet	1%	SimCLR	0.575 (0.043)	0.472 (0.022)	0.348 (0.073)	0.376 (0.070)	0.700 (0.032)	0.494 (0.048)
		BYOL	0.478 (0.086)	0.556 (0.075)	0.190 (0.075)	0.471 (0.071)	0.688 (0.011)	0.477 (0.064)
		HR-CS-CO	0.191 (0.049)	0.079 (0.039)	0.030 (0.061)	0.170 (0.070)	0.312 (0.075)	0.156 (0.059)
	5%	SimCLR	0.800 (0.009)	0.724 (0.013)	0.538 (0.087)	0.526 (0.093)	0.809 (0.004)	0.679 (0.041)
		BYOL	0.734 (0.068)	0.763 (0.035)	0.435 (0.044)	0.656 (0.047)	0.745 (0.040)	0.667 (0.047)
		HR-CS-CO	0.469 (0.056)	0.546 (0.020)	0.228 (0.051)	0.252 (0.054)	0.499 (0.036)	0.399 (0.043)
	10%	SimCLR	0.850 (0.005)	0.794 (0.017)	0.698 (0.033)	0.509 (0.077)	0.820 (0.019)	0.734 (0.030)
		HR-CS-CO	0.563 (0.051)	0.644 (0.011)	0.279 (0.016)	0.461 (0.083)	0.540 (0.034)	0.498 (0.039)
	100%	SimCLR	0.881 (0.006)	0.848 (0.016)	0.794 (0.011)	0.786 (0.024)	0.876 (0.009)	0.837 (0.013)
		BYOL	0.878 (0.007)	0.849 (0.011)	0.781 (0.012)	0.800 (0.018)	0.867 (0.011)	0.835 (0.012)
		HR-CS-CO	0.578 (0.077)	0.711 (0.009)	0.619 (0.032)	0.683 (0.028)	0.675 (0.013)	0.653 (0.032)
	MDS1	1%	SimCLR	—	0.540 (0.045)	0.348 (0.013)	0.526 (0.034)	0.513 (0.030)
BYOL			—	0.471 (0.034)	0.329 (0.029)	0.472 (0.042)	0.466 (0.026)	0.435 (0.033)
HR-CS-CO			—	0.165 (0.034)	0.085 (0.043)	0.207 (0.054)	0.186 (0.051)	0.161 (0.046)
5%		SimCLR	—	0.746 (0.013)	0.529 (0.012)	0.732 (0.012)	0.645 (0.021)	0.663 (0.014)
		BYOL	—	0.702 (0.015)	0.438 (0.020)	0.657 (0.018)	0.638 (0.022)	0.609 (0.019)
		HR-CS-CO	—	0.410 (0.014)	0.145 (0.019)	0.352 (0.014)	0.362 (0.015)	0.317 (0.015)
10%		SimCLR	—	0.806 (0.017)	0.632 (0.016)	0.731 (0.015)	0.780 (0.016)	0.709 (0.026)
		BYOL	—	0.745 (0.013)	0.612 (0.014)	0.715 (0.015)	0.729 (0.013)	0.622 (0.023)
		HR-CS-CO	—	0.435 (0.012)	0.355 (0.017)	0.482 (0.016)	0.501 (0.014)	0.365 (0.024)
100%		SimCLR	—	0.921 (0.005)	0.844 (0.010)	0.853 (0.010)	0.896 (0.010)	0.744 (0.009)
		BYOL	—	0.896 (0.008)	0.831 (0.013)	0.843 (0.010)	0.880 (0.011)	0.742 (0.015)
		HR-CS-CO	—	0.724 (0.011)	0.610 (0.016)	0.683 (0.015)	0.705 (0.013)	0.427 (0.037)
UDAGAN	1%	SimCLR	0.529 (0.038)	0.463 (0.055)	0.315 (0.078)	0.491 (0.048)	0.589 (0.043)	0.477 (0.053)
		BYOL	0.534 (0.020)	0.427 (0.018)	0.281 (0.042)	0.473 (0.051)	0.560 (0.021)	0.455 (0.031)
	5%	SimCLR	0.752 (0.007)	0.664 (0.042)	0.524 (0.067)	0.689 (0.008)	0.753 (0.010)	0.677 (0.027)
		BYOL	0.779 (0.023)	0.683 (0.043)	0.462 (0.047)	0.694 (0.026)	0.701 (0.044)	0.664 (0.037)
	10%	SimCLR	0.775 (0.019)	0.691 (0.045)	0.608 (0.035)	0.733 (0.026)	0.768 (0.011)	0.715 (0.027)
		BYOL	0.830 (0.027)	0.743 (0.029)	0.518 (0.035)	0.728 (0.031)	0.764 (0.017)	0.717 (0.028)
	100%	SimCLR	0.835 (0.018)	0.755 (0.036)	0.637 (0.056)	0.794 (0.031)	0.772 (0.032)	0.758 (0.035)
		BYOL	0.860 (0.020)	0.819 (0.022)	0.618 (0.025)	0.810 (0.022)	0.791 (0.025)	0.780 (0.023)